Preliminary aeroelastic optimization of electric aircraft wings including propeller whirl flutter effects

Wang, Zhijun; Liu Xu, Vanessa Q.; De Breuker, Roeland

Preliminary aeroelastic optimization of electric aircraft wings including propeller whirl flutter effects

Zhijun Wang *, Vanessa Q. Liu Xu, Roeland De Breuker

Faculty of Aerospace Engineering, Delft University of Technology, Kluyverweg 1, 2629 HS Delft, the Netherlands

ARTICLE INFO

ABSTRACT

In the development of electric aircraft, due to the use of Distributed Electric Propulsion (DEP), not only the classic wing flutter but also the propeller whirl flutter needs to be considered for wing structural design. To this end, this paper proposes an aeroelastic optimization method within the framework of an in-house tool named PROTEUS, which enables the preliminary design of DEP wing laminates including propeller whirl flutter effect. In this method, a new aeroelastic model is developed for the coupled propeller-wing system, based on a classic whirl flutter analysis model and the wing aeroelastic model implemented in PROTEUS. Further, the required sensitivities of aeroelastic stability constraints are derived and implemented by making use of these implemented in PROTEUS for conventional wing design. The objective of the optimization is to minimize wing mass by aeroelastically tailoring the lamination parameters and thickness of wing laminates, subject to given aerostructural design constraints. The features and usefulness of the proposed optimization approach are demonstrated through two numerical case studies (with and without whirl flutter constraints) focused on sizing the wing structure of a reference DEP aircraft. The necessary inputs regarding propeller mounting stiffness and damping for the case studies are determined through parametric studies of isolated propellers. The results indicate that including whirl flutter effect in wing sizing slightly increases wing mass, and introducing a flexible-mount-propeller leads to the decrease in wing flutter speed. Additionally, a parametric study of investigating propeller mounting stiffness is conducted, which confirms that the propeller mounting properties have a large influence on aeroelastic instability of the coupled propeller-wing system.

1. Introduction

Driven by the growing shortage of the traditional fossil energy resources and the stringent sustainability goal of reducing in-flight emissions, the concept of hybrid-electric or all-electric aircraft has garnered great attention in the past decade [1]. In contrast to the conventional aircraft powered by a fuel-based propulsion system, most electric aircraft utilize a so-called Distributed Electric Propulsion (DEP) system, where multiple electrically-driven propulsors spread across the wing span, to generate the required lift and thrust [2].

The use of DEP has a great potential to increase the aerodynamic and propulsive efficiency of the aircraft, because the propulsors can be sized, placed and operated in a beneficial manner by taking the advantages of the versatility and scalability of the electrical systems [3]. For the further improvement of aerodynamic performance, currently, most DEP aircraft concepts are equipped with high aspect ratio wings [4,5].

It is well known that thinner wings with high aspect ratio are more prone to undergo large deformations because of the higher flexibility of the wing [6,7]. This makes clearing aeroelastic instabilities, such as wing flutter, more challenging in wing design, as flexible wings tend to experience these instabilities at lower speeds compared to stiffer ones [8]. In particular, since the electric aircraft is driven by flexibly-mounted propellers, another dynamic aeroelastic instability phenomena, known as propeller whirl flutter [9,10], may occur during the operation of DEP aircraft.

Propeller whirl flutter is characterized by a diverging spiral motion described by the rotor hub, which is mainly caused by the interaction between the unsteady aerodynamic forces and moments of the propeller and the gyroscopic effects induced by the revolving rotor [11]. For propeller-driven aircraft, propeller whirl flutter and classic wing flutter can happen independently or coupled together, which can severely damage the aircraft structure on which the propeller system is mounted, and even lead to fatal accidents [12,13]. Therefore, it is important to

take both wing and propeller aeroelastic instabilities into account at the preliminary design stage of DEP aircraft.

To this end, the wing and propellers of DEP aircraft are required to be modeled as a fully-coupled system for aeroelastic analysis. This is because, on the one hand, including the flexibly-mounted and rotating propellers adds extra mass, inertia and aerodynamic loads to wing structures [5], and it also affects wing aerodynamics as the result of blowing the air around the wing [14]. On the other hand, the deformation of the flexible wing has an impact on propeller aerodynamics as it results in a change in the local angle of attack of the propeller blades [15].

Regarding to the existing studies on modeling DEP wings, Amoozgar et al. [5] have proposed an aeroelastic stability analysis method, in which the electric propellers are modeled as concentrated masses and, the propeller thrust force is included as a follower force. Although this method can account for the propeller effects on wing aeroelastic characteristics, it lacks the capability to analyze propeller whirl flutter.

In the development of the NASA X-57 Maxwell all-electric aircraft, Hoover et al. [16], Hoover and Shen [17] and Heeg et al. [18] have investigated propeller whirl flutter stability and its influence on aircraft design. Their studies are carried out by making use of the multibody dynamics simulation tools [19,20] developed for turboprop and tilt rotor aircraft [10,21,22].

Alternatively, a simple whirl flutter analysis model originally developed by Houbolt and Reed [23] recently has been reused to develop new aeroelastic analysis methods for DEP wings [24,25]. In these methods, the propeller is attached to a flexible wing via a rigid pylon considering only pitch and yaw motions. For improving the structural model of propellers, the flexibility of pylon can be accounted for using beam elements [26].

Furthermore, several sensitivity studies have been conducted based on recently developed whirl flutter analysis methods. For example, Böhnisch et al. [27,28] investigate the effects of propeller spanwise and chordwise locations, mounting stiffness, and aerodynamic interaction on aeroelastic instabilities in propeller-wing systems. Koch and Koert [29,30] propose a method to include and analyze the influence of blade elasticity on propeller whirl flutter stability, with results showing a significant stabilizing effect compared to rigid propeller blades.

Additionally, to overcome the limitations of conventional eigenvalue-based whirl flutter analysis approaches, Riso [31] explores new methods for predicting whirl flutter, such as the pre-flutter output-based bifurcation forecasting method [32] and machine learning techniques [33].

According to the literature survey, currently, only a limited number of research work has been done on the study of DEP wings considering whirl flutter instability. In particular, to the best of authors' knowledge, almost all existing studies focus on investigating the aeroelastic instabilities of the existing or given wing designs of electric aircraft. The field related to wing sizing of DEP aircraft including propeller whirl flutter effect seems to be unexplored. However, as it has been demonstrated in the development of tilt rotor aircraft [34–36], that the aeroelastic tailoring techniques are capable of reducing wing weight with the maintenance of sufficient whirl flutter stability margins.

Accordingly, the present work proposes an aeroelastic optimization method for the preliminary design of composite wings with DEP units, in which not only the classic wing aeroelastic instabilities (e.g., wing flutter) but also the propeller whirl flutter can be considered as design constraints. The proposed method is numerically implemented through extending an existing in-house tool PROTEUS [37] that is originally developed for the aeroelastic tailoring of conventional composite wings. The novelty of this paper mainly lies in developing a new aeroelastic model of the fully-coupled propeller-wing system based on the classic whirl flutter analysis model developed by Houbolt and Reed [23] and the wing aeroelastic model already implemented in PROTEUS. Further, the new sensitivities required for aeroelastic stability constraints are derived and implemented within the framework of PROTEUS, which en-

ables the optimization of DEP wing structures including propeller whirl flutter effect.

Additionally, to demonstrate the features and usefulness of the proposed optimization method, a reference DEP configuration developed in GENESIS project [38] is employed to perform numerical case studies.

The manuscript is organized as follows. In Section 2, a new aeroelastic model is developed for the coupled propeller-wing system. Section 3 provides the sensitivities required for aeroelastic stability constraints, Section 4 defines the optimization problem for the design of DEP composite wings. Then the proposed optimization method is applied to numerical case studies in Section 5. Finally, Section 6 summarizes the main conclusions of the current study.

2. Aeroelastic analysis

2.1. Wing aeroelastic model

This section reviews the wing aerodynamic and structural analysis models implemented in PROTEUS, which provides the necessary details for constructing the aeroelastic model of the coupled propeller-wing system in Section 2.3.

For wing structural analysis, a geometrically nonlinear beam Finite Element Model (FEM) is adopted. In this model, the linear Timoshenko beam elements are coupled into a co-rotational framework, making the beam model essentially nonlinear, as the stiffness properties depend on displacement [39]. In general, the structural model can be expressed as:

$$M_w \ddot{q}_w + K_w q_w = Q_w, \tag{1}$$

where q_w is composed of the degrees of freedom (DOF) of each beam node, and M_w and K_w refer to the global mass and stiffness matrices, respectively. Furthermore, Q_w represents the equivalent nodal forces and moments obtained from wing aerodynamic loads using [40]

$$Q_w = T_{AS} R_\alpha Q_w^a, \tag{2}$$

where the matrix R_α is used to rotate the wing aerodynamic loads Q_w^a through the aircraft angle of attack, α, to the body-fixed coordinate system, then the rotated wing aerodynamic loads are transferred to beam element nodes via a transformation matrix T_{AS}.

For wing aerodynamics, an unsteady vortex lattice method based on potential flow theory is implemented in PROTEUS. In this aerodynamic model, the wing aerodynamic state vector can be expressed as $x_a = [\Gamma_w^T, \alpha_{air}^T]^T$, in which the vector Γ_w contains the vortex strength of each aerodynamic panel of the free wake panels, and α_{air} are the perturbation angles of attack induced by the free stream flow. Defining $x_w = [x_a^T, x_s^T]^T$ as the aeroelastic state vector with the wing structural state vector $x_s = [\dot{q}_w^T, q_w^T]^T$, then the wing aerodynamic loads Q_w^a can be formulated as

$$Q_w^a = H_3 T_1 x_w + H_4 T_2 \dot{x}_s + L_3 B_\alpha \dot{\alpha}_{air}, \tag{3}$$

with the wing aerodynamic state equation

$$\dot{x}_a = H_1 T_1 x_w + H_2 \dot{\alpha}_{air}, \tag{4}$$

where the details on matrices H_1, H_2 H_3, H_4, T_1, T_2, L_3 and B_α can be found in Appendix B of [37]. Further details on the aerodynamic model refer to the work of Werter et al. [41].

Combining Eqs. (1) - (4), the aeroelastic state equation of the wing can be formulated as

$$\dot{x}_w = \begin{bmatrix} H_1 T_1 \\ H_5^{-1} H_6 \end{bmatrix} x_w + \begin{bmatrix} H_2 \\ H_5^{-1} H_7 \end{bmatrix} \dot{\alpha}_{air} = A_{ss} x_w + B_{ss} \dot{\alpha}_{air}, \tag{5}$$

where the formulations of the matrices H_5, H_6 and H_7 are also given in Appendix B of [37]. The aeroelastic instabilities of the classic wing (without DEP units) can be identified using the above aeroelastic model.
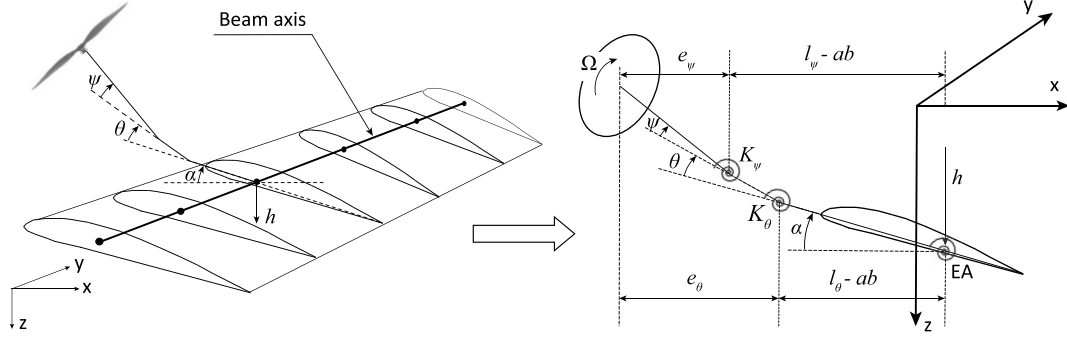
Fig. 1. Illustration of a propeller-wing model with the main parameters indicated for deriving propeller aerodynamics and equations of motion of the coupled propeller-wing system [24].

2.2. Propeller aeroelastic model

In this section, a classic whirl flutter analysis model originally developed by Houbolt and Reed [23], and recently revisited by Mair et al. [42], Liu Xu [24] and Böhnisch et al. [25], is introduced for the analysis of an isolated propeller system (which is equivalent to a propeller flexibly mounted on a rigid wing).

In the classic model, the propeller is assumed to rotate under windmilling conditions. This work considers rigid, fixed-pitch propellers, where the propeller's rotational speed changes with incoming airspeed to maintain windmilling. For constant-speed propellers, however, windmilling is achieved by adjusting the propeller blade pitch.

Further, as illustrated in Fig. 1, the motion of a flexible mounted propeller can be described using 2 DOF: Pitch θ and yaw ψ angles. For the construction of the structural dynamic model, the propeller mass is lumped into two concentrated masses: Rotor mass representing the spinner and blades and motor-nacelle system mass describing the motor, nacelle and other system components. The nacelle-pylon is simplified as a massless rigid rod with pitch and yaw pivot points (elastic centres for pitch and yaw deflections), and the rod connects the propeller concentrated masses to wing structural model, i.e., beam axis. The nacelle stiffness properties are characterized by the pitch K_θ and yaw K_ψ stiffnesses defined at pivot points. They can be determined according to the given uncoupled pitch f_θ and yaw f_ψ frequencies through $K_\theta = I_\theta (2\pi f_\theta)^2$ and $K_\psi = I_\psi (2\pi f_\psi)^2$, where I_θ and I_ψ are the propeller mass moments of inertia in pitch and yaw motions, respectively. Moreover, to evaluate the structural damping of the nacelle, the pitch g_θ and yaw g_ψ damping coefficients are required as input.

Accordingly, the equations of motion of the isolated propeller can be derived using Lagrange's equations, and the structural dynamic model of a flexibly mounted propeller can be formulated as

$$A_s \ddot{q}_p + C_s \dot{q}_p + E_s q_p = Q_p, \tag{6}$$

where $q_p = [\theta, \psi]^T$ contains the generalized coordinates of propeller, and Q_p represents propeller aerodynamic loads. The formulations of propeller mass A_s, damping C_s and stiffness E_s matrices can be found in Section 8.1.1 in [24].

The propeller aerodynamic model is built using Houbolt-Reed's method [23], where the aerodynamic loads acting on a rotating propeller are expressed via 16 aerodynamic derivatives. Accordingly, the propeller aerodynamic loads Q_p in Eq. (6) can be formulated as

$$Q_p = A_a \ddot{q}_p + C_a \dot{q}_p + E_a q_p. \tag{7}$$

Similarly, the calculation of aerodynamic mass A_a, damping C_a and stiffness E_a matrices refers to Section 8.2.1 in [24].

Inserting Eq. (7) into Eq. (6), the aeroelastic state equation of the propeller can be formulated as

$$\dot{x}_p = \begin{bmatrix} \mathbf{0} & I \\ -A_{sa}^{-1}(E_s - E_a) & -A_{sa}^{-1}(C_s - C_a) \end{bmatrix} x_p \tag{8}$$
$$= \hat{A}_{ss} x_p,$$

where $x_p = [q_p^T, \dot{q}_p^T]^T$ is the propeller structural state vector, $A_{sa} = A_s - A_a$, and I is used to represent the identical matrix throughout the paper. The above aeroelastic model is used to investigate the whirl flutter of an isolated 2-DOF propeller system.

2.3. Propeller-wing aeroelastic model

In the coupled propeller-wing system, the propeller is flexibly mounted on a flexible wing. As a consequence, the propeller displacements are not only described by pitch and yaw motions, but also have a dependency on wing deformation. As depicted in Fig. 1, in the present work, only the heave h and torsion α motions of the wing are coupled with the propeller's pitch and yaw motions, and there is no coupling between wing's inplane-bending and propeller's yaw motions. It is worth mentioning that the model illustrated in Fig. 1 is devised base on the one presented in the work of Bennett and Bland [43]. The main difference, as described in the authors' previous publication [24], is that the nodal degrees of freedom of the system are used as generalized coordinates in the present model, instead of the uncoupled vibration modes used in [43].

Applying the Lagrange's equations to the propeller that is coupled with a flexible wing, then the propeller structural dynamic model is changed from Eq. (6) to

$$A_s \ddot{q}_p + B_s \ddot{q}_{wp} + C_s \dot{q}_p + D_s \dot{q}_{wp} + E_s q_p = Q_p, \tag{9}$$

where the vector $q_{wp} = [h, \alpha]^T$ is composed of the wing nodal (vertical) displacement and twist at the section where the propeller is placed. The matrices B_s and D_s, provided in Section 8.1.1 in [24], are the new mass and damping matrices introduced for propeller model due to the coupling with the flexible wing.

Similarly, due to the coupling between propeller and wing, the propeller aerodynamic loads formulated as Eq. (7) have to be changed to

$$Q_p = A_a \ddot{q}_p + B_a \ddot{q}_{wp} + C_a \dot{q}_p + D_a \dot{q}_{wp} + E_a q_p + F_a q_{wp}, \tag{10}$$

where the aerodynamic mass B_a, damping D_a and stiffness F_a matrices are the new terms, which can be found in Section 8.2.1 in [24].

Inserting Eq. (10) into Eq. (9), then the aeroelastic model for a propeller coupled with a flexible wing can be formulated as

$$\left(A_s - A_a\right) \ddot{q}_p + \left(B_{sg} - B_{ag}\right) \ddot{q}_w + \left(C_s - C_a\right) \dot{q}_p$$
$$+ \left(D_{sg} - D_{ag}\right) \dot{q}_w + \left(E_s - E_a\right) q_p - F_{ag} q_w = \mathbf{0}, \tag{11}$$

where B_{sg}, B_{ag}, D_{sg}, D_{ag} and F_{ag} represent the global form of the matrices B_s, B_a, D_s, D_a and F_a, respectively. These global matrices are introduced as the result of replacing the vector q_{wp} by wing generalized

coordinates q_w, and they are obtained by restructuring their counterparts according to the location of the beam node that is connected to the propeller. One may refer to Appendices C and D in [24] to understand the process of coupling the propeller and wing matrices. However, note that the beam model used in [24] differs from the one used in the present work.

For a DEP wing, on one hand, including a rotating propeller adds extra mass and inertial terms into the wing structural model due to propeller mass and gyroscopic effect. On the other hand, the propeller aerodynamic loads can be added as nodal forces and moments acting on wing structural model, in order to account for the propeller aerodynamic effect on the wing. Note that the interaction between the wing and propeller aerodynamics is not considered in the present work. Accordingly, on the basis of the clean wing structural model given in Eq. (1), the dynamic structural model of a DEP wing can be formulated as

$$M_w \ddot{q}_w + K_w q_w + F_{sg} \ddot{q}_p + G_{sg} \dot{q}_w + H_{sg} \dot{q}_p = Q_w + Q_{pw}, \quad (12)$$

where F_{sg}, G_{sg} and H_{sg} are introduced because of the presence of a rotating propeller. They refer to the global form of the matrices F_s, G_s and H_s which are given in Section 8.1.1 in [24]. From the numerical implementation point of view, note that, here the global wing mass M_w and stiffness K_w matrices are obtained from PROTEUS without considering propeller concentrated masses. Moreover, Q_{pw} represents the propeller aerodynamic loads applying on wing (vertical) displacement h and twist α DOF, which can be expressed as

$$Q_{pw} = P_{1g} \ddot{q}_p + P_{2g} \ddot{q}_w + P_{3g} \dot{q}_p + P_{4g} \dot{q}_w + P_{5g} q_p + P_{6g} q_w, \quad (13)$$

where P_{1g} to P_{6g} are restructured from the matrices P_1 to P_6 that are provided in Section 8.2.2 in [24].

Combining Eqs. (11) - (13) and (2), then the dynamic structural model of the DEP wing can be formulated as

$$M_{wp} \ddot{q} + C_{wp} \dot{q} + K_{wp} q = \Phi_1 T_{AS} R_\alpha Q_w^a, \quad (14)$$

with

$$M_{wp} = \begin{bmatrix} M_w + G_{sg} - P_{2g} & F_{sg} - P_{1g} \\ B_{sg} - B_{ag} & A_s - A_a \end{bmatrix},$$

$$C_{wp} = \begin{bmatrix} -P_{4g} & H_{sg} - P_{3g} \\ D_{sg} - D_{ag} & C_s - C_a \end{bmatrix}, \quad (15)$$

$$K_{wp} = \begin{bmatrix} K_w - P_{6g} & -P_{5g} \\ -F_{ag} & E_s - E_a \end{bmatrix},$$

and $\Phi_1 = [I, 0]^T$, where the vector $q = [q_w^T, q_p^T]^T$ represents the DOF of the coupled propeller-wing system. Further, by defining $x_{wp} = [\dot{q}^T, q^T]^T$, the structural state-space system can be expressed as

$$\dot{x}_{wp} = A_{wp} x_{wp} + B_{wp} \Phi_1 T_{AS} R_\alpha Q_w^a, \quad (16)$$

where

$$A_{wp} = \begin{bmatrix} -M_{wp}^{-1} C_{wp} & -M_{wp}^{-1} K_{wp} \\ I & 0 \end{bmatrix}, \quad B_{wp} = \begin{bmatrix} M_{wp}^{-1} \\ 0 \end{bmatrix}. \quad (17)$$

To include the wing aerodynamic loads (formulated as Eq. (3)) into Eq. (16), Eq. (3) is reformulated as

$$Q_w^a = H_3 T_1 \Phi_2 x + H_4 T_2 \Phi_3 \dot{x}_{wp} + L_3 B_\alpha \dot{\alpha}_{air}, \quad (18)$$

where $x = \left[\Gamma_w^T, \alpha_{air}^T, \dot{q}_w^T, \dot{q}_p^T, q_w^T, q_p^T\right]^T$ is the state vector for the propeller-wing system, Φ_2 and Φ_3 are the matrices composed of zeros and ones, which are used to select x_w from x, $\dot{x}_s$ from $\dot{x}_{wp}$, respectively.

Subsequently, inserting Eq. (18) into Eq. (16), the aeroelastic model of the propeller-wing system can be formulated as

$$\dot{x}_{wp} = \bar{H}_5^{-1} \bar{H}_6 x + \bar{H}_5^{-1} \bar{H}_7 \dot{\alpha}_{air}, \quad (19)$$

with

$$\bar{H}_5 = I - B_{wp} \Phi_1 T_{AS} R_\alpha H_4 T_2 \Phi_3,$$

$$\bar{H}_6 = A_{wp} \Phi_4 + B_{wp} \Phi_1 T_{AS} R_\alpha H_3 T_1 \Phi_2, \quad (20)$$

$$\bar{H}_7 = B_{wp} \Phi_1 T_{AS} R_\alpha L_3 B_\alpha,$$

where Φ_4 is used to select x_{wp} from x. Combining Eqs. (4) and (19), the aeroelastic state equation of the coupled propeller-wing system can be formulated as

$$\dot{x} = \begin{bmatrix} H_1 T_1 \Phi_2 \\ \bar{H}_5^{-1} \bar{H}_6 \end{bmatrix} x + \begin{bmatrix} H_2 \\ \bar{H}_5^{-1} \bar{H}_7 \end{bmatrix} \dot{\alpha}_{air} = \bar{A}_{ss} x + \bar{B}_{ss} \dot{\alpha}_{air}, \quad (21)$$

where Φ_2 is used to select x_w from x, as mentioned above.

To identify the aeroelastic instabilities, an eigenvalue problem of the state matrix A_{ss} in Eq. (5), $\hat{A}_{ss}$ in Eq. (8), or $\bar{A}_{ss}$ in Eq. (21) is solved with the increase in airspeed, and the system is recognized as unstable when the real part of one of the eigenvalues becomes positive. Additionally, it is worthwhile to mention that the final aeroelastic model (given in Eq. (21)) derived for the coupled propeller-wing system follows a consistent form and notation used for PROTEUS wing aeroelastic model given in Eq. (5). This makes the implementation of whirl flutter analysis in PROTEUS become very straightforward. Specifically, to perform a whirl flutter analysis, the only modification in PROTEUS is to construct a new state matrix proposed in this work, which eventually only requires the inclusion of the terms introduced by propellers.

3. Sensitivity analysis

In order to govern the real part of eigenvalues of the state matrix $\bar{A}_{ss}$ in Eq. (21) to prevent the occurrence of whirl flutter and/or wing flutter, the sensitivities of the real part of eigenvalues with respect to design variables are required for optimization.

Defining an eigenvalue λ with the right u and left v eigenvectors, such that $\bar{A}_{ss} u = \lambda u$ and $v^T \bar{A}_{ss} = \lambda v^T$, then the partial derivatives of the eigenvalue λ with respect to the state matrix $\bar{A}_{ss}$ can be obtained using [44,45]

$$\frac{\partial \lambda}{\partial a_{ij}} = v^T \frac{\partial \bar{A}_{ss}}{\partial a_{ij}} u / (v^T u), \quad (22)$$

where a_{ij} refers to an element in matrix $\bar{A}_{ss}$.

According to Eqs. (20) and (21), the sensitivity of $\bar{A}_{ss}$ with respect to a design variable δ can be formulated as

$$\frac{\partial \bar{A}_{ss}}{\partial \delta} = \begin{bmatrix} \frac{\partial H_1}{\partial \delta} T_1 \Phi_2 \\ -\bar{H}_5^{-1} \frac{\partial \bar{H}_5}{\partial \delta} \bar{H}_5^{-1} \bar{H}_6 + \bar{H}_5^{-1} \frac{\partial \bar{H}_6}{\partial \delta} \end{bmatrix}, \quad (23)$$

with

$$\frac{\partial \bar{H}_5}{\partial \delta} = -\frac{\partial B_{wp}}{\partial \delta} \Phi_1 T_{AS} R_\alpha H_4 T_2 \Phi_3$$
$$- B_{wp} \Phi_1 \frac{\partial T_{AS}}{\partial \delta} R_\alpha H_4 T_2 \Phi_3 \quad (24)$$
$$- B_{wp} \Phi_1 T_{AS} R_\alpha \frac{\partial H_4}{\partial \delta} T_2 \Phi_3,$$

and

$$\frac{\partial \bar{\boldsymbol{H}}_6}{\partial \delta} = \frac{\partial \boldsymbol{A}_{\mathrm{wp}}}{\partial \delta} \boldsymbol{\Phi}_4 + \frac{\partial \boldsymbol{B}_{\mathrm{wp}}}{\partial \delta} \boldsymbol{\Phi}_1 \boldsymbol{T}_{\mathrm{AS}} \boldsymbol{R}_\alpha \boldsymbol{H}_3 \boldsymbol{T}_1 \boldsymbol{\Phi}_2$$
$$+ \boldsymbol{B}_{\mathrm{wp}} \boldsymbol{\Phi}_1 \frac{\partial \boldsymbol{T}_{\mathrm{AS}}}{\partial \delta} \boldsymbol{R}_\alpha \boldsymbol{H}_3 \boldsymbol{T}_1 \boldsymbol{\Phi}_2 \qquad (25)$$
$$+ \boldsymbol{B}_{\mathrm{wp}} \boldsymbol{\Phi}_1 \boldsymbol{T}_{\mathrm{AS}} \boldsymbol{R}_\alpha \frac{\partial \boldsymbol{H}_3}{\partial \delta} \boldsymbol{T}_1 \boldsymbol{\Phi}_2 \,,$$

where $\partial \boldsymbol{H}_1/\partial \delta$, $\partial \boldsymbol{T}_{\mathrm{AS}}/\partial \delta$, $\partial \boldsymbol{H}_3/\partial \delta$ and $\partial \boldsymbol{H}_4/\partial \delta$ are already implemented in PROTEUS for classic wing optimization. Here it is worthwhile to mention that the design variables defined in PROTEUS are the lamination parameters and laminate thickness of wing laminates. More information on the definition of wing aeroelastic optimization is given in Section 4.

Further, according to Eqs. (15) and (17), the terms $\partial \boldsymbol{B}_{\mathrm{wp}}/\partial \delta$ in Eq. (24) and $\partial \boldsymbol{A}_{\mathrm{wp}}/\partial \delta$ in Eq. (25) can be obtained via

$$\frac{\partial \boldsymbol{A}_{\mathrm{wp}}}{\partial \delta} = \begin{bmatrix} \boldsymbol{M}_{\mathrm{wp}}^{-1} \dfrac{\partial \boldsymbol{M}_{\mathrm{wp}}}{\partial \delta} \boldsymbol{M}_{\mathrm{wp}}^{-1} \boldsymbol{C}_{\mathrm{wp}} & \boldsymbol{0} \\ \boldsymbol{M}_{\mathrm{wp}}^{-1} \dfrac{\partial \boldsymbol{M}_{\mathrm{wp}}}{\partial \delta} \boldsymbol{M}_{\mathrm{wp}}^{-1} \boldsymbol{K}_{\mathrm{wp}} - \boldsymbol{M}_{\mathrm{wp}}^{-1} \dfrac{\partial \boldsymbol{K}_{\mathrm{wp}}}{\partial \delta} & \boldsymbol{0} \end{bmatrix}^{\mathrm{T}}, \qquad (26)$$

$$\frac{\partial \boldsymbol{B}_{\mathrm{wp}}}{\partial \delta} = \begin{bmatrix} -\boldsymbol{M}_{\mathrm{wp}}^{-1} \dfrac{\partial \boldsymbol{M}_{\mathrm{wp}}}{\partial \delta} \boldsymbol{M}_{\mathrm{wp}}^{-1} & \boldsymbol{0} \end{bmatrix}^{\mathrm{T}}, \qquad (27)$$

with

$$\frac{\partial \boldsymbol{M}_{\mathrm{wp}}}{\partial \delta} = \begin{bmatrix} \dfrac{\partial \boldsymbol{M}_{\mathrm{w}}}{\partial \delta} & \boldsymbol{0} \\ \boldsymbol{0} & \boldsymbol{0} \end{bmatrix}, \; \frac{\partial \boldsymbol{K}_{\mathrm{wp}}}{\partial \delta} = \begin{bmatrix} \dfrac{\partial \boldsymbol{K}_{\mathrm{w}}}{\partial \delta} & \boldsymbol{0} \\ \boldsymbol{0} & \boldsymbol{0} \end{bmatrix}, \qquad (28)$$

where $\partial \boldsymbol{M}_{\mathrm{w}}/\partial \delta$ and $\partial \boldsymbol{K}_{\mathrm{w}}/\partial \delta$ have been implemented in PROTEUS for classic wing optimization.

Since the real part of the eigenvalue λ can be implicitly expressed as $Re(\lambda) = f\left(\delta, \boldsymbol{q}_{\mathrm{w}}(\delta), \boldsymbol{x}_{\mathrm{a}}(\delta)\right)$, thus the corresponding sensitivity can be obtained by

$$\frac{d Re(\lambda)}{d \delta} = \frac{\partial Re(\lambda)}{\partial \delta} + \frac{\partial Re(\lambda)}{\partial \boldsymbol{q}_{\mathrm{w}}} \frac{d \boldsymbol{q}_{\mathrm{w}}}{d \delta} + \frac{\partial Re(\lambda)}{\partial \boldsymbol{x}_{\mathrm{a}}} \frac{d \boldsymbol{x}_{\mathrm{a}}}{d \delta}$$
$$= \frac{\partial Re(\lambda)}{\partial \bar{\boldsymbol{A}}_{\mathrm{ss}}} \left(\frac{\partial \bar{\boldsymbol{A}}_{\mathrm{ss}}}{\partial \delta} + \frac{\partial \bar{\boldsymbol{A}}_{\mathrm{ss}}}{\partial \boldsymbol{q}_{\mathrm{w}}} \frac{d \boldsymbol{q}_{\mathrm{w}}}{d \delta} + \frac{\partial \bar{\boldsymbol{A}}_{\mathrm{ss}}}{\partial \boldsymbol{x}_{\mathrm{a}}} \frac{d \boldsymbol{x}_{\mathrm{a}}}{d \delta} \right), \qquad (29)$$

where $\partial Re(\lambda)/\partial \bar{\boldsymbol{A}}_{\mathrm{ss}}$ can be determined according to Eq. (22), and $\partial \bar{\boldsymbol{A}}_{\mathrm{ss}}/\partial \delta$ is calculated using Eqs. (23)-(28). Similarly, the terms $\partial \bar{\boldsymbol{A}}_{\mathrm{ss}}/\partial \boldsymbol{q}_{\mathrm{w}}$ and $\partial \bar{\boldsymbol{A}}_{\mathrm{ss}}/\partial \boldsymbol{x}_{\mathrm{a}}$ can be also determined according to Eqs. (23)-(28) when the design variable δ is assumed to be one of elements in vector $\boldsymbol{q}_{\mathrm{w}}$ or $\boldsymbol{x}_{\mathrm{a}}$. Furthermore, the terms $d \boldsymbol{q}_{\mathrm{w}}/d \delta$ and $d \boldsymbol{x}_{\mathrm{a}}/d \delta$ are also already implemented in PROTEUS.

Note that, in principle, the derivatives of the generalized coordinates and aerodynamic derivatives of propellers with respect to design variables also need to be considered for calculating sensitivities. However, in the current work, these related terms are canceled in Eq. (29) as they are not considered for sensitivity calculation.

4. Aeroelastic optimization

In PROTEUS, composite wing structures, i.e., wing skins and spars, are divided into a series of design sections, where the independent lamination parameters and thickness assigned to each design section are defined as design variables. In the present work, the aeroelastic optimization problem defined for DEP composite wings is similar to that implemented in PROTEUS. In a general fashion, the optimization problem can be mathematically formulated as

$$\min_{\boldsymbol{V}, \bar{\boldsymbol{t}}} \quad \frac{M(\boldsymbol{V}, \bar{\boldsymbol{t}})}{M_0},$$
$$\text{subject to} \quad \frac{f_i^j(\boldsymbol{V}, \bar{\boldsymbol{t}})}{C_i^0} \le 1,$$
$$\qquad i = 1, ..., I, \quad j = 1, ..., J, \qquad (30)$$
$$\text{with} \quad -1 \le \delta \le 1,$$
$$\delta \in \{\boldsymbol{V}, \bar{\boldsymbol{t}}\},$$

where $\boldsymbol{V}$ and $\bar{\boldsymbol{t}}$ are the lamination parameters and the normalized laminate thickness of wing design sections, of which an arbitrary design variable is notated as δ. Lamination parameters are a compact representation of the stacking sequence of a laminate, their values depend solely on the stacking sequence and are independent of the material. The normalized laminate thickness is calculated using

$$\bar{t}_k = \frac{2}{U_k - L_k} \left(t_k - \frac{U_k + L_k}{2} \right), \quad k = 1, ..., K, \qquad (31)$$

where $\bar{t}_k$ represents an element of vector $\bar{\boldsymbol{t}}$, and K is the total number of wing design sections. t_k refers to the original laminate thickness, L_k and U_k are the thickness lower and upper bounds, respectively.

Similarly, the objective, i.e., wing mass M, in problem of Eq. (30) is normalized by the initial wing mass M_0. And the optimization constraints f_i^j (i-th constraint under the j-th load case) is normalized using the corresponding limit value C_i^0. Accordingly, in total, $I \times J$ constraints are considered in the optimization problem (30), in which I is the total number of constraints per load case and J is the total number of load cases.

From the numerical implementation point of view, the optimization problem of Eq. (30) is solved using the in-house tool PROTEUS. Although PROTEUS is capable of considering both static and dynamic gust loads for wing sizing [46], in this work, only the static load cases are considered for wing optimization. Furthermore, the optimization constraints cover not only aeroelastic stability, but also local angle of attack, aileron effectiveness, material strength, buckling load and lamination feasibility. Further details on design constraints in PROTEUS refer to [37] and references therein. Additionally, PROTEUS updates the design variables with the globally convergent method of moving asymptotes (GCMMA) optimizer developed by Svanberg [47].

The optimization problem of Eq. (30) can be solved using the existing version of PROTEUS for conventional wing design, where the aeroelastic stability constraints are assessed according to the aeroelastic model given in Section 2.1. However, in order to solve problem of Eq. (30) for a DEP wing including propeller whirl flutter effect, PROTEUS needs to be extended. Specifically, the aeroelastic state matrix $\boldsymbol{A}_{\mathrm{ss}}$ in Eq. (5) needs to be replaced by $\bar{\boldsymbol{A}}_{\mathrm{ss}}$ in Eq. (21). Further, the sensitivities provided in Section 3 are required to be implemented in PROTEUS for the optimization of DEP wing structures. Note that the presented optimization problems focus on investigating wing structural sizing with and without whirl flutter constraints. The aerodynamic interference between the propeller and wing, as well as propeller loads such as torque and thrust, are not considered in the optimization.

5. Numerical examples

5.1. Reference aircraft

To demonstrate the features and usefulness of the proposed optimization approach, it is applied to preliminarily design composite wing structures of a reference aircraft illustrated in Fig. 2. This DEP configuration is developed for a 50-passenger regional class hybrid-electric aircraft, one can find more details in the work of Marciello et al. [38].

As illustrated in Fig. 2, each side of the aircraft wing is equipped with five propellers, of which a thermal engine (labeled as P1) is mounted inboard and four electric engines (labeled as P2-5) are equally distributed
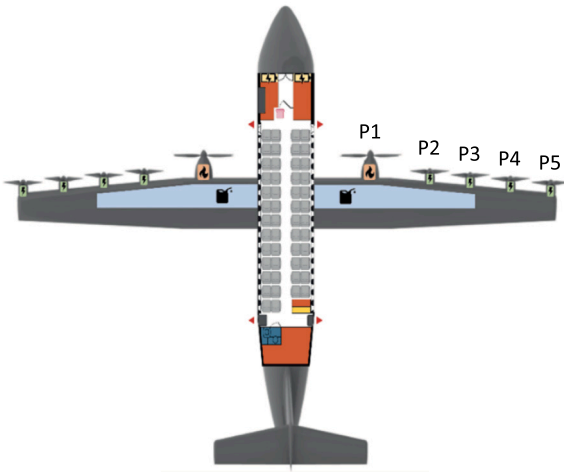
Fig. 2. Illustration of a DEP aircraft [38], where the propellers are labeled as P1-5.

Fig. 3. Structural analysis model of the DEP wing generated using in-house tool PROTEUS. (For interpretation of the colors in the figure(s), the reader is referred to the web version of this article.)

Table 3
Static load cases considered for wing structural sizing.

Load case ID	V_{EAS} (m/s)	Altitude (m)	Mach number (-)	Load factor (-)	Fuel level (-)
1	122.0	0	0.36	2.5	0.9
2	112.5	6,090	0.49	1	0.7
3	102.3	0	0.32	-1	0.5

Table 1
Main propeller parameters of the reference DEP aircraft.

Parameter	Thermal engine	Electric engine
Number of blades [-]	4	4
Blade chord [m]	0.259	0.117
Blade lift slope [rad^{-1}]	2π	2π
Geometric collective pitch angle, $\beta_{0.75R}$ [°]	25	25
Advance ratio, J [-]	1.269	1.269
Rotor radius R [m]	1.965	0.885
Hub radius [m]	0.290	0.130
Rotor mass, M_r [kg]	164	85
Motor-nacelle mass [kg]	831	336
Polar moment of inertia, I_ω [kg·m^2]	633	67

Table 2
Main characteristics of the reference aircraft wing.

Parameter	Value
Wing span [m]	24.57
Aspect ratio [-]	11.08
Planform area [m^2]	54.50
Root chord [m]	2.59
Tip chord [m]	1.39
Maximum take-off weight [kg]	23600

from semi-span to wing tip. The main propeller parameters are listed in Table 1, and note that the sole distinction among four electric engines is the mounting position. As mentioned in Section 2.2, fixed-pitch propellers are considered in this work. Accordingly, the propeller advance ratio is calculated using $J = \tan(\beta_{0.75R} - 3°)\pi$, where the geometric collective pitch angle, $\beta_{0.75R}$, is defined by the blade angle at the three-quarter radius, and $-3°$ represents the zero-lift AoA of the airfoil at the three-quarter radius. The polar moment of inertia of the propeller is estimated using $I_\omega = (M_r \cdot R^2)/3$, where M_r and R denote the rotor mass and radius, respectively.

Table 2 summarizes the main characteristics of the reference wing. Fig. 3 shows the wing structural analysis model generated using tool PROTEUS, which indicates not only the position of propeller concentrated masses (black and red dots) but also the distribution of fuel (blue square) and ribs (green dots). The static load cases considered for wing sizing are listed in Table 3.

5.2. Whirl flutter of isolated propellers

As mentioned in Section 2.2, the classic 2-DOF propeller model requires the inputs on uncoupled pitch and yaw frequencies and damping coefficients for whirl flutter analysis. In the present work, the required inputs are determined through performing parametric studies, because currently these data are not available for the reference DEP aircraft introduced in Section 5.1. It is worthwhile to mention that the uncoupled pitch and yaw frequencies can also be obtained using an optimization method, where the certification (or critical) speed is selected as input [48].

A safety factor is defined to assess the aeroelastic stability of a system. Here, the system can be an isolated propeller, a flexible wing or a coupled propeller-wing. This factor is formulated as $s = V_{\text{ins}}/(1.15V_{\text{D}})$, where V_{ins} is the approximated instability speed of the system and, $V_{\text{D}} = 1.25V_{1g}$ is the aircraft dive speed obtained according to cruise speed V_{1g}. In accordance with the load cases provided in Table 3, V_{ins} has to be equal or higher than 221.4 m/s (true airspeed) to maintain sufficient aeroelastic stability margins (i.e., $s \geq 1$).

With the prescribed values of uncoupled frequencies and damping coefficients, the whirl flutter speed of an isolated propeller can be calculated using the aeroelastic model given in Section 2.2. Accordingly, the so-called whirl flutter boundary, where $s = 1$ always holds, can be identified for each propeller via a parametric study. Note that, in this work, the pitch and yaw motions of each propeller are assumed to be symmetric, which leads to $f_\theta = f_\psi$ and $g_\theta = g_\psi$. Furthermore, it is worth mentioning that the mounting stiffnesses (represented by uncoupled pitch and yaw frequencies) are identified solely for the whirl flutter stability of the isolated engine/propeller system; no other design factors, such as the vibration isolation characteristics of the engine suspension system, are considered.

Fig. 4 depicts the whirl flutter boundaries for five isolated propellers. As shown in Fig. 4(a), the parametric study performed for thermal engine focuses on investigating the effect of damping coefficient on whirl flutter boundary. The study result indicates that, as it can be expected, the increase in nacelle structural damping enlarges the stable area. Fig. 4(b) plots the whirl flutter boundaries for four electric engines with damping coefficients $g_\theta = g_\psi = 0.005$. It can be seen that, from propeller 2 to 5, the stable region is decreased although all electric engines use the identical parameter values listed in Table 1. This trend is attributed to the monotone decrease in the distance between propeller pivot point and rotor center (i.e., propeller pivoting length), which is also indicated by the propeller mass moments of inertia given in Table 4. It is worthwhile to mention that, in this work, both the pitch and yaw pivot points are defined at wing reference axis.

(a) Thermal engine (P1)

(b) Electric engines (P2-5)
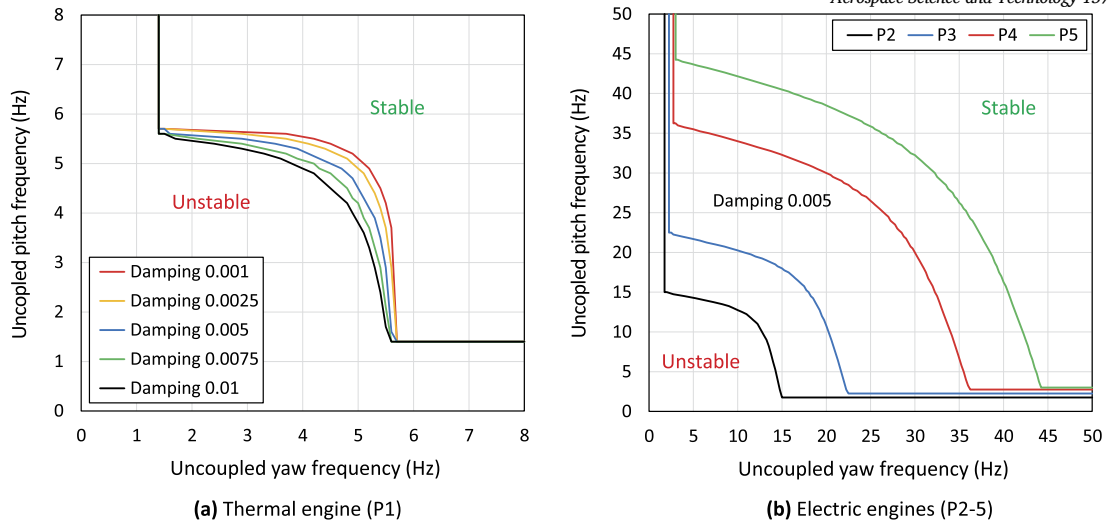
Fig. 4. Whirl flutter boundaries of the (a) thermal engine and (b) electric engines.

Table 4

Uncoupled pitch and yaw frequencies and damping coefficients chosen for each isolated propeller.

Propeller ID	P1	P2	P3	P4	P5
Uncoupled frequency [Hz] ($f_\theta = f_\psi$)	5	12	17	26	32
Damping coefficient [-] ($g_\theta = g_\psi$)	0.005	0.005	0.005	0.005	0.005
Moment of inertia [kg·m^2] ($I_\theta = I_\psi$)	4499	218	127	63	47
Stiffness [kNm/rad] ($K_\theta = K_\psi$)	4440	1239	1449	1681	1900

According to the identified whirl flutter boundaries, the uncoupled pitch and yaw frequencies of each isolated propeller listed in Table 4 are chosen to be the critical values required for providing a stable propeller system. It can be observed that, from propeller 1 to 5, the critical uncoupled frequencies are increased as the result of the decrease in propeller mass moments of inertia. Comparing the resulting pitch and yaw stiffnesses listed in Table 4, the thermal engine P1 requires higher mounting stiffness than that of electric engines P2-5 to remain stable, which is because the thermal engine is heavier than electric engines as indicated in Table 1. The comparison among four electric engines indicates that a stiffer mount is necessary when the propeller is placed closer to wing tip. This trend is similar to the finding given in the work of Houbolt and Reed [23]: A shorter propeller pivoting length requires higher nacelle stiffness to prevent whirl flutter.

Fig. 5 gives the time responses, including the pitch and yaw displacements and their velocities, of the isolated thermal engine P1. As shown in Fig. 5(a), a circle displacement path is observed due to the assumption of symmetric properties in pitch and yaw motions. Note that the motion of an isolated propeller is described by two mode shapes: backward and forward whirl mode. The backward whirl rotates in the opposite direction to the propeller rotation and, it has a lower frequency compared to the forward whirl that rotates in the same direction as the propeller rotation.

Further, only the backward whirl mode can become unstable for an isolated propeller due to the assumption of rigid wing and rotor blades. The whirl flutter rotation direction can be checked via the pitch and yaw displacements and their velocities plotted in Fig. 5(b). As it can be seen, the isolated thermal engine indeed features a backward whirl flutter as a clockwise rotation indicated by Fig. 5 is in opposite with predefined counter-clockwise propeller rotation.

5.3. Wing aeroelastic optimization

Table 5 summarizes the optimization setup for wing sizing. As introduced in Section 4, the optimization objective is to minimize wing mass

by tailoring the lamination parameters and thickness of wing laminates. In this study, the wing skins and spars are partitioned into 120 design sections. Consequently, there are in total of $120 \times 8 + 120 = 1080$ design variables.

Regarding the optimization constraints, six lamination feasibility constraints are imposed to each design section, which ensures the optimized lamination parameters always represent a feasible laminate. The composite strength failure and buckling load are assessed and restricted by means of implementing strain and buckling factors, respectively. As mentioned before, the aeroelastic stability is governed by the real part of the eigenvalues of the state matrix in aeroelastic governing equation. For efficiency, only the first 10 critical eigenvalues for each load case are restricted in this work. The constraint on minimum aileron control effectiveness is imposed for ensuring the aileron performance. In addition, the local angle of attack constraint is included to guarantee the attached aerodynamic flow. One may refer to the work of Wang et al. [46] and reference therein for more details on the aforementioned design constraints.

Table 6 lists the composite material properties used for wing sizing. Moreover, the property of aluminum alloy is chosen for modeling wing ribs and stringers.

To demonstrate the usefulness of the proposed optimization method, two optimization case studies, listed in Table 7, are defined and conducted. In *Case 1*, the wing structures are sized without considering whirl flutter constraints. Namely, the aeroelastic stability constraints are assessed using the wing model given in Section 2.1, and the effect of propellers on wing sizing is taken into account via modeling the propellers as concentrated masses. This case study can be carried out using the existing version of PROTEUS developed for conventional wing design. Based on *Case 1*, ten additional aeroelastic stability constraints for each load case, calculated using the propeller-wing model given in Section 2.3, are included in the optimization of *Case 2*. Note that solving the optimization problem in *Case 2* requires the extended PROTEUS implemented in the current work.

(a) *Pitch and yaw displacements*

(b) *Pitch and yaw displacements and velocities*
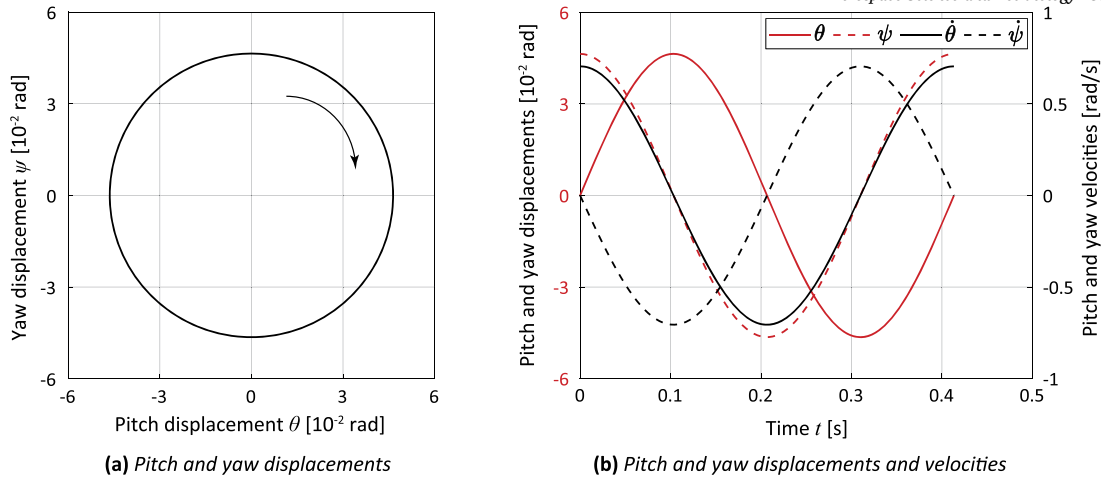
Fig. 5. Pitch and yaw displacements and their velocities of the flexibly mounted thermal engine P1 on a rigid wing.

Table 5
Aeroelastic optimization setup.

Type	Parameter	# variables	Constraint limit
Objective	Minimize wing mass	1	(-)
Design variables	Lamination parameters	$120 \times 8 = 960$	(-)
	Laminate thickness	120	(-)
Constraints	Lamination feasibility	$120 \times 6 = 720$	(-)
	Composite strength	1104 per load case	Strain factor ≤ 1
	Buckling load	7680 per load case	Buckling factor ≤ 1
	Aeroelastic stability	10 per load case	$Re(\lambda) \leq 0$
	Aileron effectiveness η	1 per load case	$\eta \geq 0.1$
	Angle of Attack AoA	34 per load case	$\lvert AoA \rvert \leq 15°$

Table 6
Composite material properties.

E_{11} (GPa)	E_{22} (GPa)	G_{12} (GPa)	v_{12} (-)	ρ (kg/m^3)	X_t (MPa)	X_c (MPa)	Y_t (MPa)	Y_c (MPa)	S (MPa)
147.0	10.3	7.0	0.27	1600	948.5	717.6	23.7	94.8	31.6

Table 7
Definition of case studies.

Case	Wing aeroelastic constraint	Whirl flutter constraint
1	Yes	No
2	Yes	Yes

For the analysis of optimization results, firstly, the objective convergence behavior and the maximum real part value (Re) of eigenvalues for aeroelastic stability constraints are plotted in Fig. 6. It shows that the wing mass at every iteration in *Case 2* is above its counterpart in *Case 1*. This is attributed to the inclusion of additional aeroelastic stability constraints, which leads to the final wing mass optimized in *Case 2* is about 2% heavier than that obtained in *Case 1*. In both *Cases 1* and *2*, the maximum Re of eigenvalues are negative throughout optimization, which means the aeroelastic stability constraints implemented for both cases are satisfied during optimization. However, when the wing design obtained in *Case 1* is reassessed using aeroelastic stability constraints implemented for the coupled propeller-wing system, the maximum Re of eigenvalues becomes positive with the reduction of wing mass (see the black line with triangle marker in Fig. 6). This demonstrates the limitation of the existing version of PROTEUS and the effectiveness of the proposed optimization method for wing sizing of DEP aircraft.

Fig. 7 provides the thickness distribution of the optimized wing structures for *Cases 1* and *2*. It shows that the thickness distribution obtained
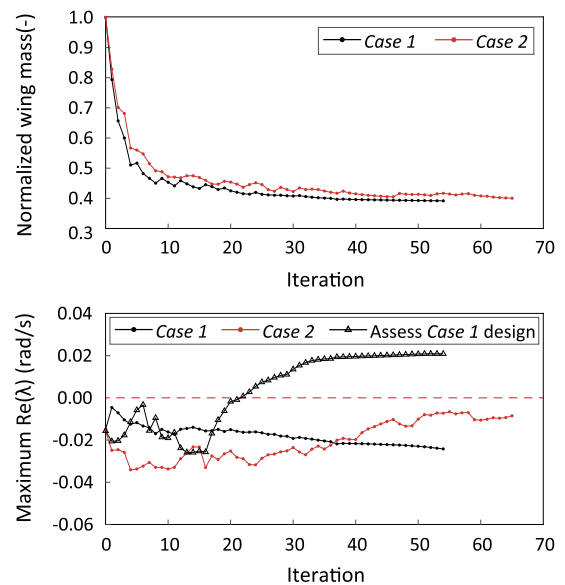
Fig. 6. Objective convergence history and the maximum real part (Re) of eigenvalues for *Cases 1* and *2*.
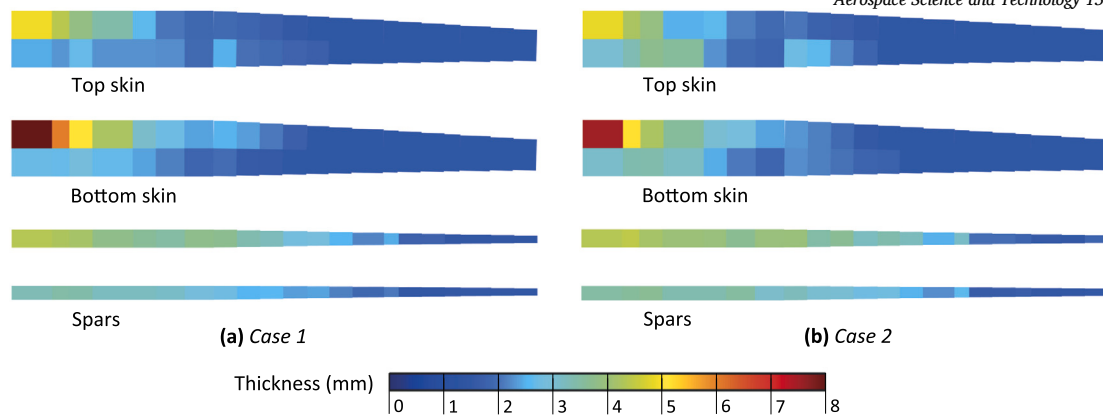
Fig. 7. Thickness distribution of the optimized wing skins and spars for *Cases 1* and *2*.
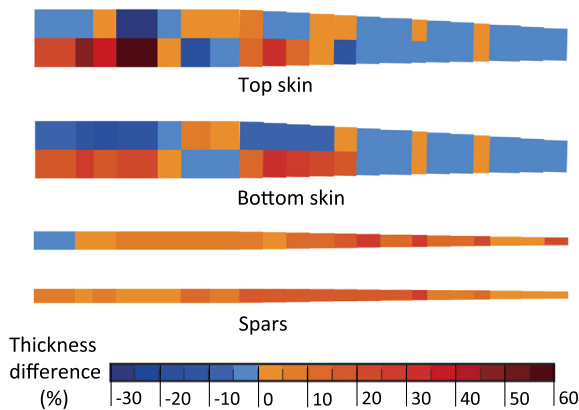
Fig. 8. Difference in thickness distribution of the optimized wing structures for *Cases 1* and *2* (*Case 2* versus *Case 1*).

in both cases follow a similar trend, where the wing root and inboard regions are thicker than other regions for carrying aerodynamic loads. Further, it can be seen that some leading edge sections are thicker than their counterparts at trailing edge. This introduces the beneficial washout effect to gain the reduction of wing mass as a result of aeroelastic tailoring. Note that, due to the limited number of load cases considered and the omission of the wing lift increase attributable to propeller aerodynamics, the optimized wing thickness is underestimated in the present work. Moreover, the difference in thickness distribution of the optimized wings (*Case 2* versus *Case 1*) is provided in Fig. 8. It can be observed that the thicknesses of most wing laminates (particularly at wing spars) are increased as the result of the additional aeroelastic stability constraints included in *Case 2*.

In order to investigate the optimized lamination parameters, Fig. 9 visualizes the laminate stiffness using a polar plot of the membrane and bending thickness-normalized modulus of elasticity. Further details on the stiffness visualization approach can be found in the work of Dillinger et al. [49] and Bordogna et al. [50]. Comparing the stiffness distributions obtained in *Cases 1* and *2*, some clear differences can be observed. These pronounced differences, along with those observed in the thickness distributions (see Fig. 8), indicate the importance of considering whirl flutter effect when sizing DEP aircraft wings.

Tables 8 and 9 list the natural frequencies of the rigid-mount-propeller wing and the flexible-mount-propeller wing for both *Cases 1* and *2*, respectively. For rigid-mount-propeller wing, aeroelastic instabilities are assessed without considering propeller DOF, which can be directly obtained from the existing version of PROTEUS. To assess the aeroelastic instabilities of the flexible-mount-propeller wing, the coupled propeller-wing aeroelastic model proposed in this work needs to be implemented in PROTEUS. The listed natural frequencies indicate

that the whirl modes of each propeller are coupled with wing modes, and this coupling has a large dependency on propeller uncoupled pitch and yaw frequencies (listed in Table 4). Moreover, it can be seen that including propeller DOF leads to the increase in the wing natural frequencies.

Table 10 gives the aeroelastic instability type, critical speed and frequency of the rigid-mount-propeller and the flexible-mount-propeller wings. It can be seen that the wing designs obtained in both *Cases 1* and *2* are safe (i.e., safety factor $s > 1$) when the propellers are rigidly mounted on the wing. Further, the wing flutter frequencies in *Cases 1* and *2*, 2.48 Hz and 2.69 Hz respectively, align with the natural frequencies of the 2nd wing mode, as listed in Tables 8 and 9 (2.43 Hz and 2.65 Hz).

Further, when the propellers are flexibly mounted on the wing, the coupled propeller-wing system obtained in *Case 1* is dangerous as the safety factor $s < 1$, while the coupled system becomes safe (i.e., safety factor $s > 1$) in *Case 2* as the result of considering additional aeroelastic stability constraints in wing sizing. In *Case 1*, the flutter frequency (25.39 Hz) is in accordance to the natural frequency (25.40 Hz) of the backward whirl mode of electric engine P5, which damages the wing system and leads to a very low (whirl) flutter speed of 38 m/s. Note that this is a specific case showing the likelihood of encountering a low flutter speed when the whirl flutter constraint is not included in wing optimization. As demonstrated in Section 5.4, the flutter speed of the propeller-wing system obtained in *Case 1* can be increased (as indicated by safety factor $s > 1$) by simply increasing the mounting stiffness (uncoupled pitch and yaw frequencies) of the propellers. In *Case 2*, the flutter frequency (8.44 Hz) aligns with the natural frequency (8.36 Hz) of the 3rd wing mode, which clearly demonstrates the effectiveness of the proposed optimization method for considering the whirl flutter effect.

Note that, theoretically, it is challenging to categorize the aeroelastic instability type in the couple propeller-wing system, because both the wing and propeller modes are present. In this work, the system instability type is categorized as *whirl flutter* when the critical frequency corresponds to a propeller whirl mode, and the category of *wing flutter* is used when the flutter frequency is in correspondence to a wing mode. Accordingly, in the current propeller-wing system, whirl flutter is recognized in *Case 1*, while wing flutter occurs in *Case 2*, as listed in Table 10. In addition, comparing the critical flutter speeds obtained with rigid and flexible mounts, it can be seen that including flexible mounts leads to the decrease in flutter speed.

5.4. Parametric study of propeller mounting stiffness

In the current work, the critical propeller mounting stiffness and damping (listed in Table 4) are used to assess aeroelastic instabilities of the given DEP wing due to the unavailability of mounting property data

(a) Membrane stiffness   Blue: *Case 1*   Red: *Case 2*   **(b)** Bending stiffness
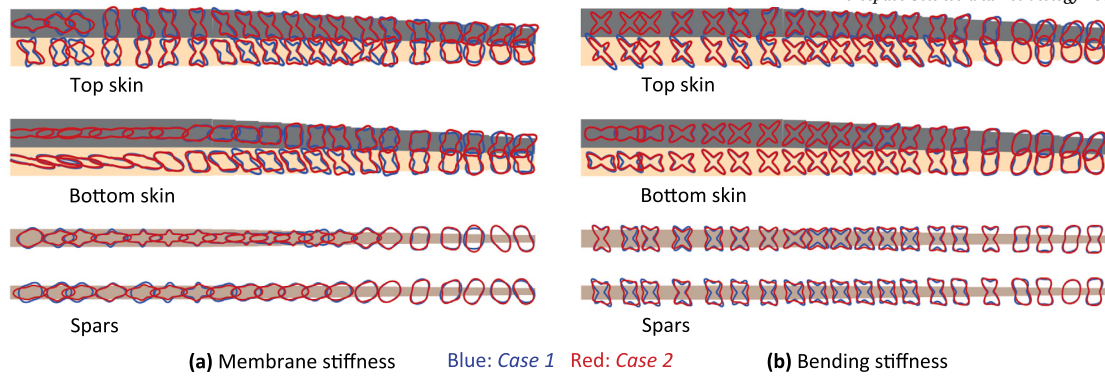
Fig. 9. Membrane (in-plane) and bending (out-of-plane) stiffness distribution of the optimized wing laminates for *Cases 1* and *2*.

Table 8
Natural frequencies of the rigid-mount-propeller wing and the flexible-mount-propeller wing for *Case 1*.

Mode	Rigid mounts [Hz]	Flexible mounts [Hz]
1st wing mode	1.08	1.17
2nd wing mode	*2.43*	4.22
Thermal engine P1 backward whirl mode	-	4.61
Thermal engine P1 forward whirl mode	-	5
3rd wing mode	3.75	7.66
Electric engine P2 backward whirl mode	-	9.48
Electric engine P2 forward whirl mode	-	12
Electric engine P3 backward whirl mode	-	13.60
Electric engine P3 forward whirl mode	-	17
Electric engine P4 backward whirl mode	-	18.37
Electric engine P5 backward whirl mode	-	*25.40*
Electric engine P4 forward whirl mode	-	26
Electric engine P5 forward whirl mode	-	32
4th wing mode	5.95	33.01
5th wing mode	8.93	35.25

Table 9
Natural frequencies of the rigid-mount-propeller wing and the flexible-mount-propeller wing for *Case 2*.

Mode	Rigid mounts [Hz]	Flexible mounts [Hz]
1st wing mode	1.11	1.20
2nd wing mode	*2.65*	4.27
Thermal engine P1 backward whirl mode	-	4.70
Thermal engine P1 forward whirl mode	-	5
3rd wing mode	3.80	*8.36*
Electric engine P2 backward whirl mode	-	9.63
Electric engine P2 forward whirl mode	-	12
Electric engine P3 backward whirl mode	-	13.73
Electric engine P3 forward whirl mode	-	17
Electric engine P4 backward whirl mode	-	18.56
Electric engine P4 forward whirl mode	-	26
Electric engine P5 backward whirl mode	-	27.39
Electric engine P5 forward whirl mode	-	32
4th wing mode	5.94	32.49
5th wing mode	9.53	33.66

Table 10
Aeroelastic instabilities of the rigid-mount-propeller wing and the flexible-mount-propeller wing.

Instability	Rigid mounts		Flexible mounts	
	Case 1	Case 2	Case 1	Case 2
Type	Wing flutter	Wing flutter	Whirl flutter	Wing flutter
Speed V_{ins} [m/s]	277	241	38	239
Frequency [Hz]	2.48	2.69	25.39	8.44
Safety factor s [-]	1.25	1.09	0.17	1.08

for real support systems. Consequently, the safety factor s may be underestimated if the propeller mounts in real designs are stiffer. Conversely, the flexible-mount-propeller wing obtained in *Case 2* could become unsafe if the mounting stiffness and/or structural damping of propellers, given in Table 4, are reduced. Accordingly, to further investigate the effect of propeller mounting properties on aeroelastic instabilities, a parametric study is conducted through varying the uncoupled propeller frequencies for the optimized wings obtained in *Cases 1* and *2*.

Fig. 10 provides the parametric study result, and it shows the trend of safety factor with the variation of uncoupled propeller pitch and yaw frequencies (listed in Table 4). Specifically, the frequency variation includes increasing or decreasing the uncoupled frequencies ($f_\theta = f_\psi$) of individual propellers (e.g., P1 and P5) and all five propellers (i.e., P1-5), ranging from 10% to 90%, respectively. In Fig. 10(a), the wing design

(a) Wing design in *Case 1*

(b) Wing design in *Case 2*
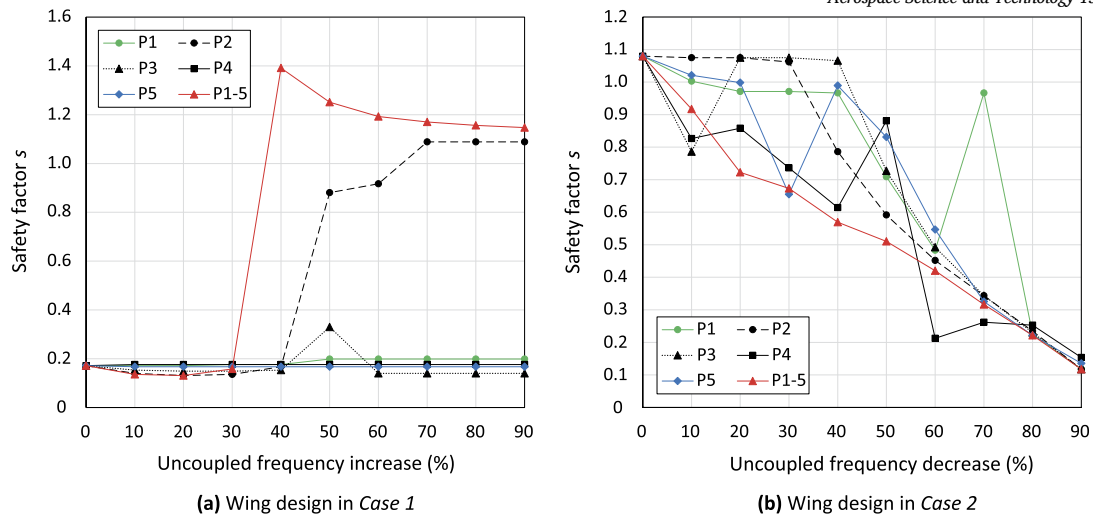
Fig. 10. Trend of safety factor with the variation of uncoupled propeller frequencies.

optimized in *Case 1* is used, and the uncoupled propeller frequencies are increased. The result shows that increasing the uncoupled frequency of the electric engine P2 by 70%, or the frequencies of all five propellers by 40% can help stabilize the couple propeller-wing system obtained in *Case 1* (i.e., safety factor $s > 1$). This demonstrates that it may be possible to fix the unsafe wing design sized without considering whirl flutter effect by increasing propeller mounting stiffness, but it still requires the development of an aeroelastic model for the fully-coupled propeller-wing system.

Further, Fig. 10(b) illustrates the trend of safety factor with reducing the uncoupled propeller frequencies for the coupled propeller-wing obtained in *Case 2*. It is clear that reducing the uncoupled frequencies of any propeller can aeroelastically destabilize the coupled system. In general, lower propeller mounting stiffness (as a result of reducing uncoupled frequencies) leads to a lower safety factor, except at specific oscillation points (e.g., P1 at 70%). When the uncoupled frequencies of all propellers are reduced at the same time, as shown by the red line with triangle marker in Fig. 10(b), the decrease in the safety factor almost follows a linear trend.

Moreover, Fig. 11 compares the flutter mode shape of the flexible-mount-propeller wing obtained in *Case 2* with the reassessed mode shape after reducing the uncoupled frequency of the thermal engine P1 by 80% (i.e., $f_\theta = f_\psi = 5\,\text{Hz} \times 0.2 = 1\,\text{Hz}$). It shows that the propeller deflection is rather small in Fig. 11(a), because the initial propeller mounting stiffness (indicated in Table 4) is sufficient, and the instability features wing flutter as indicated in Table 10. However, when the uncoupled frequencies of the thermal engine are reduced to 1 Hz, the propeller deflection is significantly increased, as can be observed in Fig. 11(b). In this case, the instability type of the coupled propeller-wing system is categorized as whirl flutter, where the backward whirl mode of the thermal engine P1 is very pronounced.

In summary, the parametric study results confirm that the propeller mounting properties have a large influence on aeroelastic instability of the coupled propeller-wing system. This effect, in this study, is demonstrated through altering only uncoupled propeller frequencies, but it also will be interesting to perform parametric studies on propeller mounting damping and pivoting length, as indicated in the work of Liu Xu [24]. Further, the optimization method developed in this work focuses on realizing wing structural sizing with prescribed propeller properties. Accordingly, it is recommended to further develop the presented aeroelastic optimization method by including propeller mounting effect in future work.

Additionally, although the in-house tool, PROTEUS, has been numerically verified against other tools [37], such as NASTRAN [51], further verification of the extended version of the PROTEUS using a benchmark

(a) $f_\theta = f_\psi = 5$ Hz

(b) $f_\theta = f_\psi = 1$ Hz
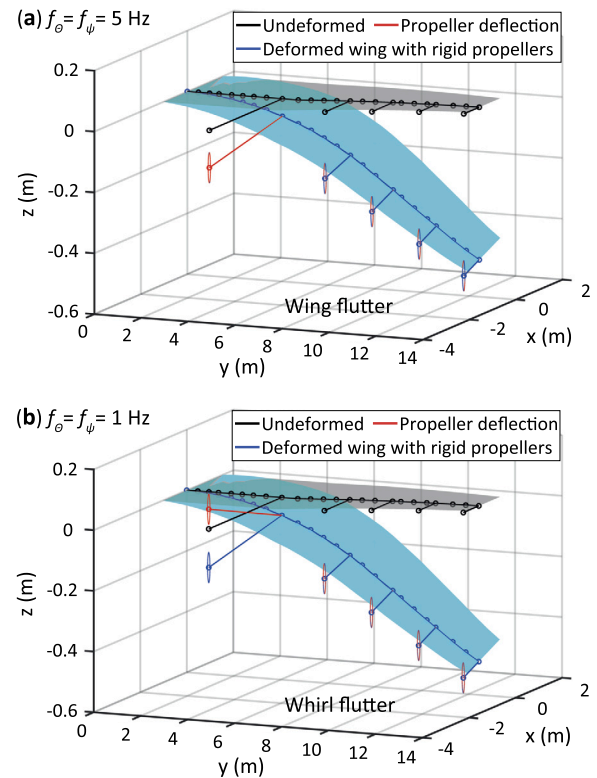
Fig. 11. Flutter mode shape of the coupled propeller-wing obtained in *Case 2* with different uncoupled frequencies of the thermal engine P1.

DEP wing remains a valuable direction for future work. Specifically, enhancing PROTEUS to include functionality for categorizing system modes could enable a more detailed investigation of the instability mechanisms in the coupled propeller-wing system. This improvement would further strengthen the proposed method in analyzing and optimizing DEP wing configurations.

6. Conclusions

This work proposes and implements a new aeroelastic optimization method within the framework of an in-house tool named PROTEUS, which enables the consideration of propeller whirl flutter for the preliminary design of DEP aircraft wings. In the proposed method, a classic

whirl flutter analysis model, in which the pitch and yaw motions are considered to describe propeller DOF, is coupled to the conventional wing aeroelastic model implemented in PROTEUS, to build an aeroelastic model of the fully-coupled propeller-wing system. The developed aeroelastic model is formulated into a state-space form, so that the instabilities of DEP wings can be identified by analyzing the eigenvalues of the state matrix. Further, to consider the whirl flutter effect in wing sizing, the constraints on state matrix eigenvalues are included in an aeroelastic optimization model formulated for minimizing wing mass. Additionally, the sensitivity of the whirl flutter constraint is derived analytically based on the existing wing aeroelastic sensitivities implemented in PROTEUS.

The developed optimization method has been applied to two case studies in the preliminary wing design of a DEP configuration developed in GENESIS project, which demonstrates the usefulness of the proposed method. In the present case studies, wing mass is minimized by aeroelastically tailoring the lamination parameters and thicknesses of wing laminates, subject to the design constraints on wing and propeller aeroelastic stability, aileron effectiveness, material strength and buckling load. The required inputs of propeller uncoupled frequency and damping for whirl flutter analysis are determined by performing a parametric study of isolated propellers. The results of case studies indicate that considering whirl flutter effect in wing sizing slightly increases the optimized wing mass, and including flexible propeller mounts leads to the decrease in wing flutter speed. Moreover, a parametric study has been conducted to investigate the impact of propeller mounting stiffness on aeroelastic instabilities, where the uncoupled propeller frequencies used for the wing designs obtained in case studies varied from 10% to 90%. The result confirms that the propeller mounting properties have a large influence on aeroelastic instability of the coupled propeller-wing system. Accordingly, it is recommended to incorporate the effects of propeller mounting properties into the proposed aeroelastic optimization method in future work.

CRediT authorship contribution statement

Zhijun Wang: Writing – original draft, Visualization, Validation, Software, Methodology, Investigation, Formal analysis, Data curation, Conceptualization. **Vanessa Q. Liu Xu:** Writing – review & editing, Software, Resources, Methodology. **Roeland De Breuker:** Writing – review & editing, Supervision, Project administration, Methodology, Funding acquisition, Conceptualization.

Declaration of competing interest

The authors declare that they have no known competing financial interests or personal relationships that could have appeared to influence the work reported in this paper.

Acknowledgements

Data availability

Data will be made available on request.

References

[1] B.J. Brelje, J.R.R.A. Martins, Electric, hybrid, and turboelectric fixed-wing aircraft: a review of concepts, models, and design approaches, Prog. Aerosp. Sci. 104 (2019) 1–19.

[2] H.D. Kim, A.T. Perry, P.J. Ansell, A review of distributed electric propulsion concepts for air vehicle technology, in: 2018 AIAA/IEEE Electric Aircraft Technologies Symposium (EATS), IEEE, 2018, pp. 1–21.

[3] R. de Vries, R. Vos, Aerodynamic performance benefits of over-the-wing distributed propulsion for hybrid-electric transport aircraft, in: AIAA SCITECH 2022 Forum, 2022, p. 0128.

[4] J.B. Moore, S. Cutright, Structural design exploration of an electric powered multi-propulsor wing configuration, in: 58th AIAA/ASCE/AHS/ASC Structures, Structural Dynamics, and Materials Conference, 2017, p. 0203.

[5] M. Amoozgar, M.I. Friswell, S.A. Fazelzadeh, H. Haddad Khodaparast, A. Mazidi, J.E. Cooper, Aeroelastic stability analysis of electric aircraft wings with distributed electric propulsors, Aerospace 8 (2021) 100.

[6] F. Afonso, J. Vale, É. Oliveira, F. Lau, A. Suleman, Non-linear aeroelastic response of high aspect-ratio wings in the frequency domain, Aeronaut. J. 121 (2017) 858–876.

[7] X. Wang, W. Zhou, R. Mu, Z. Wu, A new deformation control approach for flexible wings using moving masses, Aerosp. Sci. Technol. 106 (2020) 106118.

[8] F. Afonso, J. Vale, É. Oliveira, F. Lau, A. Suleman, A review on non-linear aeroelasticity of high aspect-ratio wings, Prog. Aerosp. Sci. 89 (2017) 40–57.

[9] W.H. Reed III, Propeller-rotor whirl flutter: a state-of-the-art review, J. Sound Vib. 4 (1966) 526–544.

[10] D.L. Kunz, Analysis of proprotor whirl flutter: review and update, J. Aircr. 42 (2005) 172–178.

[11] A. Quintana, B.E. Saunders, R. Vasconcellos, A. Abdelkefi, Nonlinear characterization of the piecewise structural effects on whirl flutter of a rotor-nacelle system, in: AIAA SCITECH 2022 Forum, 2022, p. 2269.

[12] F.T. Abbott Jr, H.N. Kelley, K.D. Hampton, Investigation of propeller-power-plant autoprecession boundaries for a dynamic-aeroelastic model of a four-engine turbo-prop transport airplane, Technical Report, NASA, 1963.

[13] R.E. Donham, G.A. Watts, Lessons learned from fixed and rotary wing dynamic and aeroelastic encounters, in: 41st Structures, Structural Dynamics, and Materials Conference and Exhibit, 2000, p. 1599.

[14] K.A. Deere, J.K. Viken, S.A. Viken, M.B. Carter, M. Wiese, N. Farr, Computational analysis of a wing designed for the X-57 distributed electric propulsion aircraft, in: 35th AIAA Applied Aerodynamics Conference, 2017, p. 3923.

[15] P. Aref, M. Ghoreyshi, A. Jirasek, M.J. Satchell, K. Bergeron, Computational study of propeller–wing aerodynamic interaction, Aerospace 5 (2018) 79.

[16] C.B. Hoover, J. Shen, A.R. Kreshock, Propeller whirl flutter stability and its influence on X-57 aircraft design, J. Aircr. 55 (2018) 2169–2175.

[17] C.B. Hoover, J. Shen, Parametric study of propeller whirl flutter stability with full-span model of X-57 Maxwell aircraft, J. Aircr. 55 (2018) 2530–2537.

[18] J. Heeg, B.K. Stanford, A. Kreshock, J. Shen, C.B. Hoover, R. Truax, Whirl flutter and the development of the NASA X-57 Maxwell, in: International Forum on Aeroelasticity and Structural Dynamics, NF1676L-31615, 2019.

[19] W. Johnson, Technology drivers in the development of CAMRAD II, in: American Helicopter Society Aeromechanics Specialists Conference, San Francisco, California, 1994.

[20] O.A. Bauchau, C.L. Bottasso, Y.G. Nikishkov, Modeling rotorcraft dynamics with finite element multibody procedures, Math. Comput. Model. 33 (2001) 1113–1137.

[21] J. Cecrdle, Whirl Flutter of Turboprop Aircraft Structures, Woodhead Publishing, 2015.

[22] H. Yeo, A.R. Kreshock, Whirl flutter investigation of hingeless proprotors, J. Aircr. 57 (2020) 586–596.

[23] J.C. Houbolt, W.H. Reed, Propeller-nacelle whirl flutter, J. Aerosp. Sci. 29 (1962) 333–346.

[24] V.Q. Liu Xu, Propeller-Wing Whirl Flutter: An Analytical Approach, Delft University of Technology, 2020.

[25] N. Böhnisch, C. Braun, S. Koschel, P. Marzocca, Whirl flutter for distributed propulsion systems on a flexible wing, in: AIAA SCITECH 2022 Forum, 2022, p. 1755.

[26] C. Koch, Parametric whirl flutter study using different modelling approaches, CEAS Aeronaut. J. (2021) 1–11.

[27] N. Böhnisch, C. Braun, V. Muscarello, P. Marzocca, A sensitivity study on aeroelastic instabilities of slender wings with a large propeller, in: AIAA SCITECH 2023 Forum, 2023, p. 1893.

[28] N. Böhnisch, C. Braun, P. Marzocca, V. Muscarello, Impact of aerodynamic interactions on aeroelastic stability of wing-propeller systems, Appl. Sci. 14 (2024) 8709.

[29] C. Koch, B. Koert, Influence of blade elasticity on propeller whirl flutter stability, in: AIAA SCITECH 2023 Forum, 2023, p. 1307.

[30] C. Koch, B. Koert, Including blade elasticity into frequency-domain propeller whirl flutter analysis, J. Aircr. 61 (2024) 774–784.

[31] C. Riso, Output-based prediction of whirl flutter limit-cycle oscillations considering multiple varying parameters, in: AIAA SCITECH 2024 Forum, 2024, p. 1847.

[32] S.V. Gali, T.G. Goehmann, C. Riso, Fundamental investigation into output-based prediction of whirl flutter bifurcations, J. Fluids Struct. 123 (2023) 103986.

[33] M. Gatlin, C. Riso, Predicting whirl flutter bifurcations using machine learning, in: 80th VFS Annual Forum, Montreal, Canada, 2024, pp. 1–15.

[34] J.-S. Park, S.N. Jung, M.-K. Lee, J.M. Kim, Design optimization framework for tiltrotor composite wings considering whirl flutter stability, Composites, Part B, Eng. 41 (2010) 257–267.

[35] J. Zhang, E.C. Smith, Advanced composite wings for whirl flutter augmentation: wind tunnel model design, in: 56th AIAA/ASCE/AHS/ASC Structures, Structural Dynamics, and Materials Conference, 2015, p. 1414.

[36] S. Kambampati, E.C. Smith, Aeroelastic optimization of high-speed tiltrotor wings with wing extensions and winglets, J. Aircr. 54 (2017) 1718–1727.

[37] N.P.M. Werter, R. De Breuker, A novel dynamic aeroelastic framework for aeroelastic tailoring and structural optimisation, Compos. Struct. 158 (2016) 369–386.

[38] V. Marciello, M. Di Stasio, M. Ruocco, V. Trifari, F. Nicolosi, M. Meindl, B. Lemoine, P. Caliandro, Design exploration for sustainable regional hybrid-electric aircraft: a study based on technology forecasts, Aerospace 10 (2023) 165.

[39] R. De Breuker, M.M. Abdalla, Z. Gürdal, A generic morphing wing analysis and design framework, J. Intell. Mater. Syst. Struct. 22 (2011) 1025–1039.

[40] N.P.M. Werter, Aeroelastic modelling and design of aeroelastically tailored and morphing wings, Ph.D. thesis, Delft University of Technology, 2017.

[41] N.P.M. Werter, R. De Breuker, M.M. Abdalla, Continuous-time state-space unsteady aerodynamic modeling for efficient loads analysis, AIAA J. 56 (2018) 905–916.

[42] C. Mair, D. Rezgui, B. Titurus, Nonlinear stability analysis of whirl flutter in a rotor-nacelle system, Nonlinear Dyn. 94 (2018) 2013–2032.

[43] R.M. Bennett, S.R. Bland, Experimental and analytical investigation of propeller whirl flutter of a power plant on a flexible wing, Technical Report, 1964.

[44] D.V. Murthy, R.T. Haftka, Survey of methods for calculating sensitivity of general eigenproblems, in: NASA. Langley Research Center Sensitivity Analysis in Engineering, 1987.

[45] P. Lancaster, On eigenvalues of matrices dependent on a parameter, Numer. Math. 6 (1964) 377–387.

[46] Z. Wang, D. Peeters, R. De Breuker, An aeroelastic optimisation framework for manufacturable variable stiffness composite wings including critical gust loads, Struct. Multidiscip. Optim. 65 (2022) 290.

[47] K. Svanberg, A class of globally convergent optimization methods based on conservative convex separable approximations, SIAM J. Optim. 12 (2002) 555–573.

[48] J. Čečrdle, Whirl flutter optimisation-based solution of twin turboprop aircraft using a full-span model, Appl. Comput. Mech. 11 (2017).

[49] J.K.S. Dillinger, T. Klimmek, M.M. Abdalla, Z. Gürdal, Stiffness optimization of composite wings with aeroelastic constraints, J. Aircr. 50 (2013) 1159–1168.

[50] M.T. Bordogna, P. Lancelot, D. Bettebghor, R. De Breuker, Static and dynamic aeroelastic tailoring with composite blending and manoeuvre load alleviation, Struct. Multidiscip. Optim. (2020) 1–24.

[51] X. Carrillo Córcoles, R. De Breuker, J. Sodja, Aeroelastic tailoring of a strut-braced wing for a medium range aircraft, in: AIAA SCITECH 2024 Forum, 2024, p. 2590.